CTRC Research Publications   Cooling Technologies Research Center

2020

On the Transient Thermal Response of Thin Vapor Chamber Heat Spreaders: Optimized Design and Fluid Selection

G. Patankar

J. A. Weibel

S V. Garimella

On the Transient Thermal Response of Thin Vapor Chamber Heat Spreaders: Optimized Design and Fluid Selection

Gaurav Patankar, Justin A. Weibel and Suresh V. Garimella[*,1]

Cooling Technologies Research Center
School of Mechanical Engineering, Purdue University
585 Purdue Mall, West Lafayette, IN 47907 USA

Abstract

Vapor chambers provide highly effective heat spreading to assist in the thermal management of electronic devices. Although there is a significant body of literature on vapor chambers, most prior research has focused on their steady-state response. In many applications, electronic devices generate inherently transient heat loads and, hence, it is critical to understand the transient thermal response of vapor chambers. We recently developed a semi-analytical transport model that was used to identify the key mechanisms that govern the thermal response of vapor chambers to transient heat inputs (Int. J. Heat Mass Trans. 136 (2019) 995–1005). The current study utilizes this understanding of the governing mechanisms to develop design guidelines for improving the performance of vapor chambers under transient operating conditions. Two key aspects of vapor chamber design are addressed in this study: first, a parametric optimization of the wall, wick, and vapor-core thicknesses; and second, the selection of the working fluid. A protocol is demonstrated for selecting these parameters given the external vapor chamber envelope dimensions and boundary conditions. The study helps provide a framework for designing vapor chambers subject

---

[*] Corresponding author: Tel. 765 494 5621 ; sureshg@purdue.edu
[1] Currently President, University of Vermont

to transient heat loads, and to differentiate such design from the practices followed traditionally for steady-state operation.

Keywords: transient, vapor chamber, heat pipe, design, working fluid

Nomenclature

C_p	specific heat capacity [J kg^{-1} K^{-1}]
C_{vol}	volumetric heat capacity of the liquid phase [J m^{-3} K^{-1}]
h	convection coefficient [W m^{-2} K^{-1}]
h_{fg}	specific enthalpy of vaporization [J kg^{-1}]
K	permeability [m^2]
k	thermal conductivity [W m^{-1} K^{-1}]
M_l	liquid-phase figure of merit
M_v	vapor-phase figure of merit
$\dot{m}''$	mass flux rate [kg m^{-2} s^{-1}]
P	pressure [Pa]
Q	input power [W]
R	specific gas constant [J kg^{-1} K^{-1}]
T	temperature [K]
T_{sat}	saturation temperature [K]
T_∞	ambient temperature [K]
t	time [s]
u	x-component of velocity [m s^{-1}]

2

$\vec{V}$	velocity vector [m s^{-1}]
v	y-component of velocity [m s^{-1}]
w	z-component of velocity [m s^{-1}]
x	x-coordinate (length) direction [m]
y	y-coordinate (width) direction [m]
z	z-coordinate (thickness) direction [m]

Greek

δ_{vap}	vapor-core thickness [m]
δ_{wick}	wick thickness [m]
δ_{wall}	wall thickness [m]
θ	temperature relative to the ambient (T-T_∞) [K]
μ	viscosity [Pa s]
ρ	density [kg m^{-3}]
σ	accommodation coefficient [-]
ϕ	porosity [-]

Subscript

eff	effective wick property
int	wick–vapor interface
l	liquid phase
m	volume-averaged
p	evaporator maximum
p-m	difference between evaporator maximum and volume-averaged values

3

v   vapor phase

1. Introduction

A vapor chamber is a passive heat spreading device driven by the change of phase of an internal working fluid. A typical vapor chamber comprises a sealed metal chamber with a porous wick lining its inner surface. The chamber is evacuated and charged with a working fluid; the porous wick holds the liquid phase of the fluid, while the core is occupied by vapor. The working principle of a vapor chamber is illustrated in Figure 1. A localized heat input on the so-called evaporator surface leads to evaporation at the adjacent wick-vapor interface, causing vapor to flow away from the source and to condense at the opposing colder wick-vapor interface, rejecting heat to the condenser surface. The condensed liquid is pulled back towards the heat input region due to the capillary action of the porous wick.

Effective thermal management of electronic devices has enabled their continual advance towards higher heat loads and heat densities. The highly effective heat spreading capabilities of vapor chambers have resulted in significant research being conducted for their use in a wide range of applications, from high heat fluxes (> 500 Wcm^{-2}) such as in radar power amplifiers and high-performance computing systems, to low-power (< 10 W) mobile electronic devices [1]. Space constraints and transient heat loads are common among these applications. For example, mobile devices operate at very low power in an idle state but experience pulses of higher power while using applications such as video calling. Additionally, the compact shape of these devices means that only submillimeter-thick volumes are available for heat spreading.

Previous work in the literature for the design of vapor chambers has focused on improving performance at steady state [2-10]. To inform these design approaches, studies have identified the key mechanisms governing the vapor chamber performance at steady-state conditions. Prasher *et al.* [11] developed a resistance-network representation of heat pipes, where the transport processes

5

in the wall, wick, and vapor core are represented by analogous thermal resistances. The model revealed that the performance of a vapor chamber for high power applications is limited by the resistance across the wick near the evaporator. Significant research has focused on designing the evaporator wick for reducing its resistance during evaporation or capillary-fed boiling [5-10, 12-19]. Recent work by Yadavalli *et al.* [20]identified that the performance of ultra-thin vapor chambers dissipating low powers is limited by the thermal resistance in the vapor core. Based on this limiting resistance, our previous studies have developed methods for design of vapor chambers [4] and selection of working fluids [21]for ultra-thin form factors and low-power operation.

The thermal behavior of vapor chambers under transient operation has also been studied. El-Genk and Lianmin [22] conducted experiments to study the heat-up and cool-down of heat pipes for a range of heat inputs and condenser coolant flow rates. They concluded that the transient vapor temperature profiles could be locally represented by an exponential function in the cases tested. Tournier and El-Genk [23] developed a model that simulated the transient mass, momentum, and energy transport in a vapor chamber using the finite-volume method to study the pooling of liquid in the condenser. Zhu and Vafai [24] developed an analytical model to solve for heat spreading from a centrally located heater in disk- and rectangular-shaped vapor chambers. The model solved 1D transient conduction in the wall and the wick, while the quasi-steady vapor-core hydrodynamics was computed by assuming a spatial velocity profile. The model was then used to simulate the startup behavior of the transient vapor chamber temperature and velocity fields. Harmand *et al.* [25] developed a model for transient transport in a vapor chamber using the finite-volume method. The model was validated against experiments and subsequently the capabilities of the model were demonstrated for a range of scenarios with multiple heat sources and sinks. However, these and other [2629-30] analyses in the literature did not attempt to extract any

6

guidelines or procedures to design vapor chambers for improved performance during transient operation.

In our recent work [31] , a low-cost, 3D, transient semi-analytical transport model [32] was used to identify the key mechanisms governing the transient thermal behavior of vapor chambers; the occurrence of these mechanisms was confirmed with experiments. Knowing these key mechanisms, we develop a protocol for the design of vapor chambers under transient heat loading in the current work. Two key aspects of the vapor chamber design are considered: (1) optimization of the thicknesses of the vapor chamber wall, wick, and vapor core, for a given total available thickness; and (2) selection of the working fluid for a given set of boundary conditions. Simulations performed with the time-stepping analytical model [32] are used to identify and demonstrate a procedure for designing the vapor chamber.

2. Model and simulation case details

2.1 Time-stepping analytical model for vapor chamber transport

The time-stepping analytical model [32] is used for simulating the transient response of vapor chambers in this work. This transient 3D transport model is applicable for the rectangular geometries of the vapor chamber wall, wick, and vapor core, configured such that the wick lines the inner surface of the wall and encloses the vapor core as shown in Figure 1. The boundary conditions for the model can be arbitrarily shaped and located heat inputs on either of the faces, with the remaining face area being insulated or exposed to convection. All of the boundary conditions can vary in time, given the transient nature of the model. The mass, momentum, and energy transport are solved in the wall, wick, and vapor core of the vapor chamber. The phase

7

change process is simulated at the wick-vapor interface. The model outputs are 3D transient fields of temperature, pressure and velocity.

The governing equations for the mass, momentum, and energy transport, before simplification, are given below.

$$\frac{\partial u}{\partial x} + \frac{\partial v}{\partial y} + \frac{\partial w}{\partial z} = 0 \tag{1}$$

$$\rho \frac{\partial \vec{V}}{\partial t} + \rho \left(u \frac{\partial \vec{V}}{\partial x} + v \frac{\partial \vec{V}}{\partial y} + w \frac{\partial \vec{V}}{\partial z} \right)$$
$$= -\nabla(\phi P) + \mu \left(\frac{\partial^2 \vec{V}}{\partial x^2} + \frac{\partial^2 \vec{V}}{\partial y^2} + \frac{\partial^2 \vec{V}}{\partial z^2} \right) - \frac{\mu \phi}{K} \vec{V} \tag{2}$$

$$(\rho C_P)_{eff} \left(\frac{\partial T}{\partial t} \right) + (\rho C_P)_l \left(u \frac{\partial T}{\partial x} + v \frac{\partial T}{\partial y} + w \frac{\partial T}{\partial z} \right)$$
$$= k_{eff} \left(\frac{\partial^2 T}{\partial x^2} + \frac{\partial^2 T}{\partial y^2} + \frac{\partial^2 T}{\partial z^2} \right) \tag{3}$$

In the vapor core, the porosity ϕ is set to 1 and the permeability K is set to ∞, whereas in the wick region these values take on the properties of the wick. In the wick region, k_{eff} is the effective conductivity, while in the wall and vapor core, k_{eff} is the material thermal conductivity. The fluid volumetric heat capacity in the wick and vapor core, $(\rho C_P)_l$, is set to zero in the wall region. The effective volumetric heat capacity of the three regions is given by:

for the wick, $(\rho C_P)_{eff} = \phi(\rho C_P)_l + (1-\phi)(\rho C_P)_s$,

for the wall, $(\rho C_P)_{eff} = (\rho C_P)_{wall}$, and

for the vapor core, $(\rho C_P)_{eff} = (\rho C_P)_{vap}$,

The mass flux rate due to phase change at the wick–vapor interface is computed using the difference between the local interface temperature and the local vapor-core saturation temperature [33] as:

$$\dot{m}'' = \frac{2\sigma}{2-\sigma} \frac{h_{fg}\rho_{vap}}{T_{vap}^{1.5}} \left(\frac{1}{2\pi R}\right)^{0.5} \left(T_{int} - T_{sat}\right).$$ (4)

The saturation temperature in the vapor core is computed using the Clausius-Clapeyron equation

$$\frac{dP_{vap}}{dT_{sat}} = \frac{h_{fg}P_{vap}}{RT_{sat}^2}.$$ (5)

The model simplifies the governing equations using scaling analysis and assumed temperature profiles along the thickness, to allow solution at a low computational cost [32]. The final set of differential equations (see [32]) are solved analytically in space and numerically in time. It is important to note that using a numerical solution in time allows for the use of temperature-dependent thermophysical properties for the vapor phase, which can change considerably over the typical operating temperatures; the fluid properties are computed at each time step based on the volume-averaged temperature. In our recent work [31], the model was validated against experiments.

This time-stepping analytical model allows a large number of cases to be evaluated over a wide range of design parameters at a tractable computational cost. Simulations are run using a custom script that implements the model in the commercial software MATLAB [34].

2.2. Simulation case details

Details of the vapor chamber simulations used for demonstrating the vapor chamber design procedures are described here. The geometry and boundary conditions for the simulations are shown in Figure 2. The rectangular vapor chamber has a length of 80 mm, a width of 60 mm, and a thickness of 300 μm. The vapor chamber wall is made of copper and the wick of sintered copper.

9

The temperature-dependent properties of the working fluid are obtained from the commercial fluid database software REFPROP [35]. The relevant properties of the wick and copper are included in Table 1Table 1.

The vapor chamber is subjected to a heat input of 4 W starting at time $t = 0$ over an area of 10 mm × 10 mm at the center of the evaporator-side face. The rest of the evaporator-side face is insulated. The opposite face has a convective boundary condition, with heat transfer coefficient h = 30 Wm^{-2}K^{-1} and ambient temperature T_∞ = 300 K. At time $t = 0$, the vapor chamber is initially at a temperature of 300 K. Two time-step sizes are used for time-marching, 0.05 s for $t < 10$ s and 1 s for $t > 10$ s.

3. Optimization of the wall and vapor-core thicknesses

As discussed in Ref. [31], the total thermal capacity of the vapor chamber is effectively the sum of the thermal capacities of the wall and the wick, and hence will increase with an increase in wall or wick thickness. The effective in-plane vapor-core conductance increases with an increase in the vapor-core thickness. The wick has a minimum thickness requirement to satisfy the capillary limit; thicknesses below this minimum value would result in higher flow velocities with the attendant pressure drop exceeding the capillary pressure. For a fixed overall thickness, and setting the wick to its minimum thickness, an increase in the vapor-core thickness will increase the effective in-plane conductance of the vapor core, but reduce the wall thickness and hence the total thermal capacity. Although both the wick and the wall provide thermal capacity for the vapor chamber, it is always favorable to minimize the wick thickness. This is because both the wall and wick have similar values of volumetric capacity (3420.6 kJm^{-3}K^{-1} for copper and 4166.3 kJm^{-3}K^{-1} for liquid water), but a copper wall has a much higher conductivity than a porous wick.

10

Based on this tradeoff, an optimization of the vapor-core and wall thicknesses is clearly necessary; for a fixed external geometry and set of boundary conditions, vapor chambers with a range of wall and vapor-core thicknesses are simulated to identify the optimum allotment between these two thicknesses. The factors governing these optimum values are compared under transient versus steady-state conditions.

Water is selected as the working fluid for these simulations. The value for the accommodation coefficient σ (equation 4) is set to 0.03 [36]. The thickness of the wick layers on either side is set to 10 μm, which is the minimum value needed to avoid encountering the capillary limit at the selected heat input level. The thickness of the wall on either side is varied from 10 μm to 130 μm; within the total available thickness, the vapor-core thickness correspondingly varies from 260 μm to 20 μm. Note that a minimum wall thickness is needed to support the pressure difference between the internal vapor and the external atmosphere; evaluation of this mechanical limit is beyond the scope of this study.

Figure 3a shows the temporal profile of the temperature, θ_p, at the center of the heat input area relative to the ambient temperature, for three values of vapor-core thickness. The value of θ_p for each of the three cases increases from 0 at $t = 0$ toward a steady-state value. At steady state ($t = 200$ s), the peak temperature θ_p is highest for the smallest vapor-core thickness, and the value monotonically decreases as the vapor-core thickness is increased from 20 μm to 100 μm to 260 μm. The highest temperature in the vapor chamber is at the evaporator, and this value is typically used for characterizing vapor chamber performance. Under transient conditions, given that this temperature is time-varying, multiple methods can be used to characterize performance (e.g., the time for θ_p to reach a set maximum limit, the value of θ_p at a particular time, or an average value of θ_p over a range of time). In this study, the transient performance of the vapor chamber is

11

characterized by the peak temperature θ_p at time $t = 50$ s (marked by the vertical dashed line in Figure 3a). At time $t = 50$ s, θ_p reduces from 31 K to 26.1 K when the vapor-core thickness is increased from 20 μm to 100 μm but then increases to 28.6 K when the vapor-core thickness is further increased to 260 μm. Thus, we observe that the relation between the vapor-core thickness (and by extension the wall thickness) and the transient performance is nonmonotonic, unlike the monotonic relationship at steady state.

To understand this relationship between the transient performance and the vapor-core thickness, the peak temperature θ_p is decomposed into two components, the mean (volume-averaged) temperature θ_m, shown in Figure 3b, and the difference between the peak and mean temperatures, $\Delta\theta_{p-m} = \theta_p - \theta_m$ (*i.e.*, the peak-to-mean difference), shown in Figure 3c. As identified in our previous work [31], three mechanisms govern the transient thermal behavior of vapor chambers: 1) the *total thermal capacity* of the vapor chamber governs the rate of increase of the volume-averaged mean temperature, θ_m; 2) the *effective in-plane conductance* of the vapor core governs the magnitude of the peak-to-mean temperature difference, $\Delta\theta_{p-m}$; 3) the *effective in-plane diffusivity* governs the time required for the initial rise in the peak-to-mean temperature difference $\Delta\theta_{p-m}$. The third mechanism is only relevant for a brief initial period ($t < 10$ s, as seen in Figure 3c), and thus, is not relevant for this specific investigation of performance at 50 s. For the fixed wick thickness considered, the total thermal capacity of the vapor chamber decreases with increasing vapor-core thickness (and corresponding reduction in wall thickness). Thus, in Figure 3b, the vapor chamber heats up faster with increasing vapor-core thickness and the value of θ_m at time $t = 50$ s monotonically increases. As discussed in Ref. [31], the effective in-plane conductance of the vapor core increases polynomially with increasing vapor-core thickness. As seen in Figure 3c, the peak-to-mean temperature difference $\Delta\theta_{p-m}$ is smaller at all times for the larger vapor-core

12

thicknesses. Thus, the two mechanisms governing the transient vapor chamber performance (at t = 50 s) have opposite trends with vapor-core thickness, leading to the net nonmonotonic relationship observed in Figure 3a. Note that at steady state, the total thermal capacity of the vapor chamber is irrelevant, and the performance is only governed by the effective in-plane conductance of the vapor core, which explains the monotonic improvement in vapor chamber performance at steady state (at t = 200 s) with increasing vapor-core thickness.

Figure 4a and Figure 4b respectively show the vapor chamber steady-state (at t = 200 s) and transient (at t = 50 s) evaporator temperature θ_p as a function of the vapor-core thickness. At steady state (Figure 4a), the performance monotonically improves (*i.e.*, the temperature decreases) with increasing vapor-core thickness. To design a vapor chamber for improved steady-state performance, the vapor-core thickness should generally be maximized, as proposed in our previous work [4]. However, under transient conditions, due to the nonmonotonic dependence of performance on the vapor-core thickness, an optimum value of the vapor-core thickness exists that minimizes θ_p, at 90 μm in this case. Thus, when designing a vapor chamber for improved transient performance, the optimal ratio between the vapor-core thickness and wall thickness must be evaluated for the specific case and operating time of interest. Traditional vapor chamber design practices developed in the past based on the steady-state performance metrics cannot be directly adopted for design under transient conditions.

4. Selection of working fluid

4.1 Selection procedure

The performance of a vapor chamber is sensitive to the thermophysical properties of both the liquid and vapor phases of the working fluid. Therefore, selecting a working fluid is critical to the

design of a vapor chamber. In our previous work [21], the relationship between the properties of the working fluid and the steady-state performance of a vapor chamber was identified, and a procedure developed that allows selection of the working fluid that provides the best steady-state performance among available options. Two fluid property groups govern the performance of a vapor chamber at steady state, the liquid-phase figure of merit M_l and the vapor-phase figure of merit M_v, defined as

$$M_l = \frac{\gamma \rho_l h_{fg}}{\mu_l} \quad \text{and} \quad M_v = \frac{P_v \rho_v h_{fg}^2}{\mu_v R T_v^2}. \tag{6}$$

The liquid figure of merit M_l has been commonly used for the selection of working fluids that maximize the capillary limit in conventional vapor chambers having a relatively thick vapor core [37]. At the capillary limit, the pressure drop in the liquid matches the capillary pressure provided by the porous wick; any increase in the liquid pressure drop beyond this value would result in dryout of the wick near the evaporator. The properties included in the liquid-phase figure of merit thereby govern the required wick thickness to avoid the capillary limit, at a given operating power. The vapor figure of merit, introduced by Yadavalli *et al.* [20], governs the effective in-plane conductance of the vapor core.

A procedure for the selection of working fluids to minimize the evaporator peak temperature at steady state was defined in Ref. [21]. As discussed in Section 3, the steady-state performance of a vapor chamber is maximized by maximizing the vapor-core thickness. Thus, for a fixed total thickness of the vapor chamber, minimizing the wick and wall thicknesses maximizes the vapor-core thickness. The minimum required thickness of the wick to avoid the capillary limit is computed as a function of M_l ($\delta_{wick} \propto M_l^{-0.5}$). The maximized vapor-core thickness and M_v

14

determine the effective in-plane conductance of the vapor core. The fluid that yields the highest effective in-plane conductance of the vapor core is selected as the working fluid.

The performance of a vapor chamber under transient conditions, on the other hand, is governed by both the total thermal capacity of the vapor chamber, including the thermal capacities of the wick and the wall, and the effective in-plane conductance of the vapor core. The thermal capacities of the wall and wick are governed by their thicknesses and material specific heat capacities; in the case of the wick, the heat capacity is directly related to the volumetric capacity of the liquid phase of the working fluid, C_{vol}. The effective in-plane conductance of the vapor core is governed by the vapor-core thickness and M_v. The following procedure is proposed for selection of the working fluid that maximizes performance under transient conditions (*i.e.*, minimizes the evaporator temperature at a given time) for a given case. For each candidate working fluid: 1) minimize the thickness of the wick to satisfy the capillary limit based on the M_l value for the fluid; 2) optimize the thicknesses of the wall and vapor core as discussed in Section 3; this fluid-specific optimization is governed by the tradeoff between increasing the total thermal capacity of the wall and decreasing the effective in-plane conductivity of the vapor core. This procedure can be repeated for all fluids of interest to identify the one that yields the best performance.

4.2 Demonstration of the procedure

The procedure for the selection of the working fluid is demonstrated in this section for the case described in Section 2.2. This demonstration is conducted to choose between two working fluids, water and methanol. The thermophysical properties of the fluids are obtained from the commercial fluid database software REFPROP [35] and the values of the relevant property groups are shown in Table 2Table 2, computed at a temperature of 300 K. The value for the accommodation coefficient σ (equation 4) is set to 0.03 for water [36] and 0.056 for methanol [38].

15

The first step in the working fluid selection procedure is to minimize the wick thickness for the given operating power. The minimum wick thickness is found to be 10 μm for water and 23 μm for methanol, which follows an inverse proportionality with the square root of M_l, as noted in Section 4.1. The second step is to optimize between the wall and the vapor-core thicknesses. For methanol, the thickness of the wall is varied from 10 μm to 120 μm. The vapor-core thickness correspondingly varies from 234 μm to 14 μm. The variations explored for water are the same cases as those described above in Section 3.

Figure 5 shows the evaporator temperature θ_p as a function of vapor-core thickness for the two fluids. The plot shows that the optimum vapor-core thickness for the two fluids is different, being 90 μm (95 μm wall thickness) for water compared to 52 μm (101 μm wall thickness) for methanol. More importantly, at these optimum dimensions, the value of θ_p for methanol (24.1 K) is lower than that for water (26.1 K). This can be attributed to the improved total thermal capacity and effective in-plane conductance for the optimal design with methanol as the working fluid. The wall and wick thicknesses are both larger with methanol, leading to a higher total thermal capacity, despite the lower volumetric capacity of methanol compared to water. This is indicated by the lower value of θ_m (23.3 K) as compared to that for the case with water (24.1 K). The effective in-plane conductance is governed by the vapor-core thickness and M_v. For the case with methanol, despite a much smaller vapor-core thickness, the significantly higher value of M_v leads to a smaller value of $\Delta\theta_{p-m}$ (0.8 K) than with water (2.0 K).

The relationships between the design parameters and the vapor chamber performance are complex and nonintuitive. The procedural approach developed here allows for rational design of vapor chambers for transient conditions. Although the procedure is demonstrated here for specific cases, it is based on an understanding of the mechanisms governing the general transient thermal

16

behavior of vapor chambers. The procedure can therefore generally be applied for a broad range of operating conditions, including different geometries, boundary conditions, and transient metrics.

5. Conclusions

In this work, guidelines are developed for the design of vapor chambers to improve their performance under transient conditions, which include an optimization of the thicknesses of the wall, the wick, and the vapor core, and the selection of a working fluid. A procedural approach is developed for the design of these parameters, followed by a demonstration using simulations of representative cases. The procedures are informed by the key mechanisms governing the nonintuitive transient thermal behavior of vapor chambers. It was concluded that the traditional practices for optimization of the vapor chamber wall, wick, and vapor-core thicknesses under steady-state conditions, cannot be directly used under transient conditions. Due to the existence of multiple governing mechanisms, with sometimes competing effects, the design of vapor chambers under transient conditions must be evaluated for the specific case and operating time of interest. The procedural approach developed here can be generally applied to user-specific cases of interest, as it accounts for the multiple governing mechanisms that determine vapor chamber transient performance.

17

References

[1] J. A. Weibel and S. V. Garimella, "Recent Advances in Vapor Chamber Transport Characterization for High-Heat-Flux Applications," in Advances in Heat Transfer, vol. 45, pp. 209–301, 2013.

[2] C. Ding, G. Soni, P. Bozorgi, B. D. Piorek, C. D. Meinhart, and N. C. MacDonald, "A Flat Heat Pipe Architecture Based on Nanostructured Titania," Journal of Microelectromechanical Systems, vol. 19, no. 4, pp. 878–884, 2010.

[3] R. Lewis, S. Xu, L. Liew, C. Coolidge, R. Yang, and Y. Lee, "Thin Flexible Thermal Ground Planes: Fabrication and Scaling Characterization," Journal of Microelectromechanical Systems, vol. 24, no. 6, pp. 2040–2048, 2015.

[4] G. Patankar, J. A. Weibel, and S. V. Garimella, "Patterning the Condenser-Side Wick in Ultra-Thin Vapor Chamber Heat Spreaders to Improve Skin Temperature Uniformity of Mobile Devices," International Journal of Heat and Mass Transfer, vol. 101, pp. 927–936, 2016.

[5] Y. Zhao and C.-L. Chen, "An Investigation of Evaporation Heat Transfer in Sintered Copper Wicks with Microgrooves," in ASME International Mechanical Engineering Congress and Exposition, Chicago, IL, USA, pp. 177–181, 2006.

[6] T. Semenic and I. Catton, "Experimental Study of Biporous Wicks for High Heat Flux Applications," International Journal of Heat and Mass Transfer, vol. 52, no. 21–22, pp. 5113–5121, 2009.

[7] J. A. Weibel and S. V. Garimella, "Visualization of Vapor Formation Regimes during Capillary-Fed Boiling in Sintered-Powder Heat Pipe Wicks," International Journal of Heat and Mass Transfer, vol. 55, no. 13–14, pp. 3498–3510, 2012.

[8] Y. S. Ju, M. Kaviany, Y. Nam, S. Sharratt, G. S. Hwang, I. Catton, E. Fleming, and P. Dussinger, "Planar Vapor Chamber with Hybrid Evaporator Wicks for the Thermal Management of High-Heat-Flux and High-Power Optoelectronic Devices," International Journal of Heat and Mass Transfer, vol. 60, pp. 163–169, 2013.

[9]   Y. Peng, W. Liu, B. Liu, J. Liu, K. Huang, L. Wang, and W. Chen, "The Performance of the Novel Vapor Chamber Based on the Leaf Vein System," International Journal of Heat and Mass Transfer, vol. 86, pp. 656–666, 2015.

[10] S. Sudhakar, J. A. Weibel, and S. V. Garimella, "Design of an Area-Scalable Two-Layer Evaporator Wick for High-Heat-Flux Vapor Chambers," IEEE Transactions on Components, Packaging and Manufacturing Technology, pp. 1–1, 2018.

[11] R. S. Prasher, "A Simplified Conduction Based Modeling Scheme for Design Sensitivity Study of Thermal Solution Utilizing Heat Pipe and Vapor Chamber Technology," Journal of Electronic Packaging, vol. 125, no. 3, pp. 378–385, 2003.

[12] G. S. Hwang, Y. Nam, E. Fleming, P. Dussinger, Y. S. Ju, and M. Kaviany, "Multi-Artery Heat Pipe Spreader: Experiment," International Journal of Heat and Mass Transfer, vol. 53, no. 13–14, pp. 2662–2669, 2010.

[13] J. A. Weibel, S. V. Garimella, and M. T. North, "Characterization of Evaporation and Boiling from Sintered Powder Wicks Fed by Capillary Action," International Journal of Heat and Mass Transfer, vol. 53, no. 19–20, pp. 4204–4215, 2010.

[14] Q. Cai and Y.-C. Chen, "Investigations of Biporous Wick Structure Dryout," Journal of Heat Transfer, vol. 134, no. 2, pp. 021503–021503, 2011.

[15] D. Ćoso, V. Srinivasan, M.-C. Lu, J.-Y. Chang, and A. Majumdar, "Enhanced Heat Transfer in Biporous Wicks in the Thin Liquid Film Evaporation and Boiling Regimes," Journal of Heat Transfer, vol. 134, no. 10, p. 101501, 2012.

[16] A. S. Kousalya, J. A. Weibel, S. V. Garimella, and T. S. Fisher, "Metal Functionalization of Carbon Nanotubes for Enhanced Sintered Powder Wicks," International Journal of Heat and Mass Transfer, vol. 59, pp. 372–383, 2013.

[17] J. W. Palko, C. Zhang, J. D. Wilbur, T. J. Dusseault, M. Asheghi, K. E. Goodson, and J. G. Santiago, "Approaching the Limits of Two-Phase Boiling Heat Transfer: High Heat Flux and Low Superheat," Applied Physics Letters, vol. 107, no. 25, p. 253903, 2015.

[18] T. Liu, S. Lingamneni, J. Palko, M. Asheghi, and K. E. Goodson, "Optimization of Hybrid Wick Structures for Extreme Spreading in High Performance Vapor Chambers," in 15th IEEE Intersociety Conference on Thermal and Thermomechanical Phenomena in Electronic Systems, Las Vegas, NV, USA, pp. 30–36, 2016.

[19] M. R. Shaeri, D. Attinger, and R. W. Bonner, "Vapor Chambers with Hydrophobic and Biphilic Evaporators in Moderate to High Heat Flux Applications," Applied Thermal Engineering, vol. 130, pp. 83–92, 2018.

[20] Y. Yadavalli, J. A. Weibel, and S. V. Garimella, "Performance-Governing Transport Mechanisms for Heat Pipes at Ultrathin Form Factors," IEEE Transactions on Components, Packaging and Manufacturing Technology, vol. 5, no. 11, pp. 1618–1627, 2015.

[21] G. Patankar, J. A. Weibel, and S. V. Garimella, "Working-Fluid Selection for Minimized Thermal Resistance in Ultra-Thin Vapor Chambers," International Journal of Heat and Mass Transfer, vol. 106, pp. 648–654, 2017.

[22] M. S. El-Genk and H. Lianmin, "An Experimental Investigation of the Transient Response of a Water Heat Pipe," International Journal of Heat and Mass Transfer, vol. 36, no. 15, pp. 3823–3830, 1993.

[23] J.-M. Tournier and M. S. El-Genk, "A Heat Pipe Transient Analysis Model," International Journal of Heat and Mass Transfer, vol. 37, no. 5, pp. 753–762, 1994.

[24] N. Zhu and K. Vafai, "Vapor and Liquid Flow in an Asymmetrical Flat Plate Heat Pipe: A Three-Dimensional Analytical and Numerical Investigation," International Journal of Heat and Mass Transfer, vol. 41, no. 1, pp. 159–174, 1998.

[25] S. Harmand, R. Sonan, M. Fakès, and H. Hassan, "Transient Cooling of Electronic Components by Flat Heat Pipes," Applied Thermal Engineering, vol. 31, no. 11–12, pp. 1877–1885, 2011.

[26] U. Vadakkan, S. V. Garimella, and J. Y. Murthy, "Transport in Flat Heat Pipes at High Heat Fluxes from Multiple Discrete Sources," Journal of Heat Transfer, vol. 126, no. 3, pp. 347–354, 2004.

[27] Y. Xuan, Y. Hong, and Q. Li, "Investigation on Transient Behaviors of Flat Plate Heat Pipes," Experimental Thermal and Fluid Science, vol. 28, no. 2–3, pp. 249–255, 2004.

[28] S. Murer, P. Lybaert, L. Gleton, and A. Sturbois, "Experimental and Numerical Analysis of the Transient Response of a Miniature Heat Pipe," Applied Thermal Engineering, vol. 25, no. 16, pp. 2566–2577, 2005.

[29] R. Sonan, S. Harmand, J. Pellé, D. Leger, and M. Fakès, "Transient Thermal and Hydrodynamic Model of Flat Heat Pipe for the Cooling of Electronics Components," International Journal of Heat and Mass Transfer, vol. 51, no. 25–26, pp. 6006–6017, 2008.

[30] M. Famouri, M. M. Abdollahzadeh, A. Abdulshaheed, G. Huang, G. Carbajal, and C. Li, "Transient Analysis of a Cylindrical Heat Pipe Considering Different Wick Structures," in ASME Heat Transfer Summer Conference, p. V002T08A023, 2016.

[31] G. Patankar, J. A. Weibel, and S. V. Garimella, "On the Transient Thermal Response of Thin Vapor Chamber Heat Spreaders: Governing Mechanisms and Performance Relative to Metal Spreaders," vol. 136, pp. 995-1005, 2019.

[32] G. Patankar, J. A. Weibel, and S. V. Garimella, "A Validated Time-Stepping Analytical Model for 3D Transient Vapor Chamber Transport," International Journal of Heat and Mass Transfer, vol. 119, pp. 867–879, 2018.

[33] V. P. Carey, Liquid-Vapor Phase-Change Phenomena. Washington (D.C.), USA: Hemisphere Pub. Corp, 1992.

[34] MATLAB Release 2017a. Natick, Massachusetts, United States: The MathWorks, Inc.

[35] E. W. Lemmon, M. L. Huber, and M. O. McLinden, NIST Standard Reference Database 23: Reference Fluid Thermodynamic and Transport Properties-REFPROP. Gaithersburg: National Institute of Standards and Technology, Standard Reference Data Program, 2013.

[36] R. Marek and J. Straub, "Analysis of the Evaporation Coefficient and the Condensation Coefficient of Water," International Journal of Heat and Mass Transfer, vol. 44, no. 1, pp. 39–53, 2001.

[37] P. D. Dunn and D. A. Reay, "The Heat Pipe," Physics in Technology, vol. 4, no. 3, p. 187, 1973.

[38] J. T. Jayne, S. X. Duan, P. Davidovits, D. R. Worsnop, M. S. Zahniser, and C. E. Kolb, "Uptake of Gas-Phase Alcohol and Organic Acid Molecules by Water Surfaces," The Journal of Physical Chemistry, vol. 95, no. 16, pp. 6329–6336, 1991.

21

List of Figures

List of Tables

23

Table 1. Copper and wick properties.

Property	Value
Wick effective thermal conductivity (k_{eff})	40 $\text{Wm}^{-1}\text{K}^{-1}$
Copper volumetric thermal capacity $\left(\rho C_P \right)_s$	3.42×10^6 $\text{Jm}^{-3}\text{K}^{-1}$
Wick porosity (ϕ)	0.6
Copper thermal conductivity (k)	387.6 $\text{Wm}^{-1}\text{K}^{-1}$

Table 2. Fluid property figures of merit for water and methanol.

Property	Water	Methanol
M_l (/10^{10}) (Wm^{-2})	20.4	3.8
M_v (/10^{12}) (Wm^{-3}K^{-1})	1.3	27.7
C_{vol} (/10^{6}) (Jm^{-3}K^{-1})	4.2	2.0
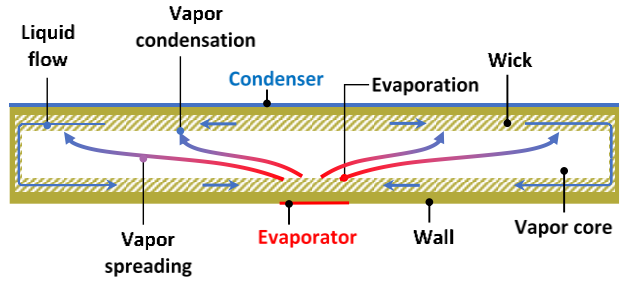
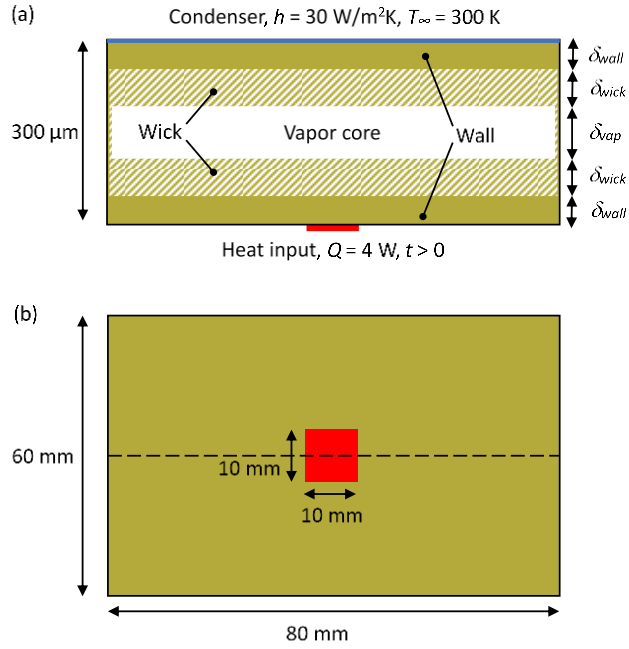Figure 1. Illustration of the typical internal layout and operation of a vapor chamber.

Figure 2. Geometry (not to scale) and boundary conditions for the transient vapor chamber simulations showing (a) a section view, and (b) a bottom view of the evaporator side.
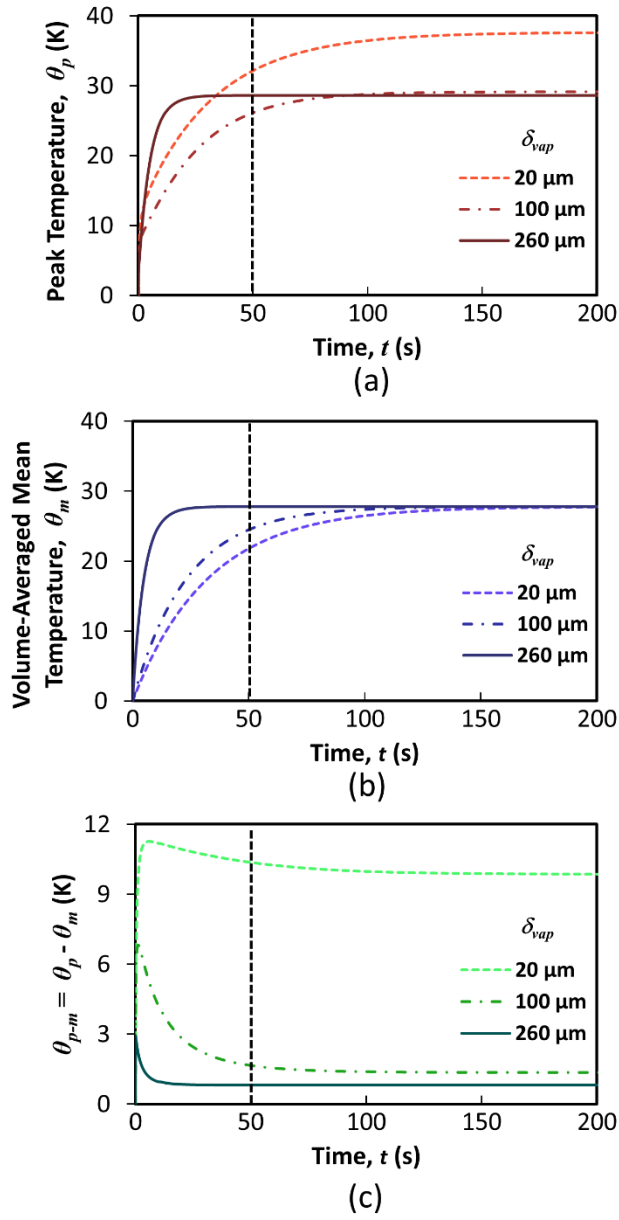
Figure 3. Transient response of a vapor chamber for multiple values of vapor-core thickness, showing the temporal variation of the (a) peak temperature θ_p, (b) volume-averaged mean temperature θ_m, and (c) difference between the peak and mean temperatures $\Delta\theta_{p-m} = \theta_p - \theta_m$.
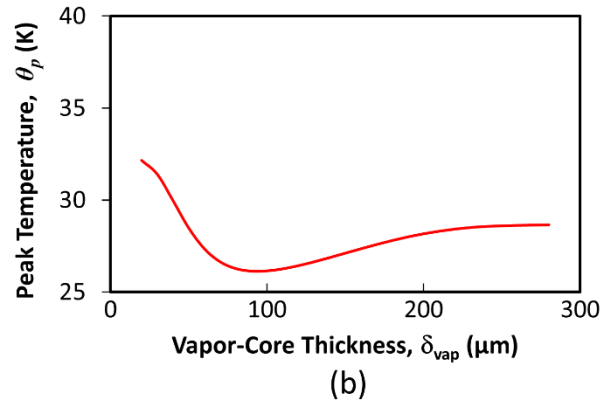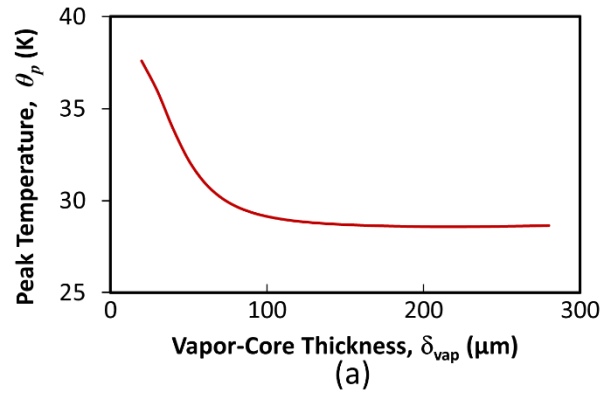
Figure 4. Vapor chamber peak temperature θ_p as a function of vapor-core thickness δ_{vap} (a) at steady state ($t = 200$ s), and (b) at $t = 50$ s.
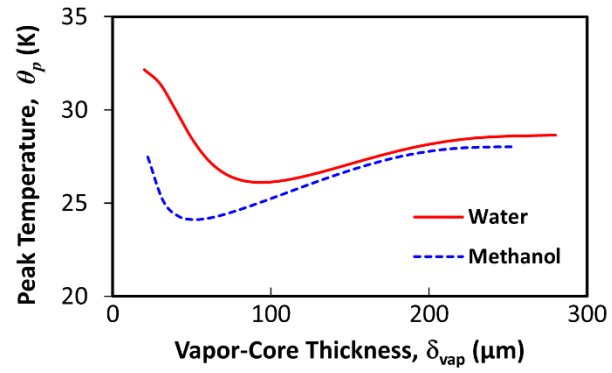
29

Figure 5. Selection of working fluid by comparing the vapor chamber peak temperature θ_p as a function of vapor-core thickness δ_{vap} for water and methanol as working fluids, under transient conditions ($t = 50$ s).